

**Recent Developments in Three Dimensional Radiation Transport  
using the Green's Function Technique**

Candice Rockell<sup>1,\*</sup>, John Tweed<sup>1</sup>, Steve R. Blattnig<sup>2</sup> and Christopher J. Mertens<sup>2</sup>

<sup>1</sup> *Old Dominion University, Norfolk, VA 23529*

<sup>2</sup> *NASA Langley Research Center, Hampton, VA 23681-2199*

\* *Corresponding author: [crockell@odu.edu](mailto:crockell@odu.edu)*

Number of pages: 25

Number of tables: 0

Number of figures: 8

## **ABSTRACT**

*In the future, astronauts will be sent into space for longer durations of time compared to previous missions. The increased risk of exposure to dangerous radiation, such as Galactic Cosmic Rays and Solar Particle Events, is of great concern. Consequently, steps must be taken to ensure astronaut safety by providing adequate shielding. In order to better determine and verify shielding requirements, an accurate and efficient radiation transport code based on a fully three dimensional radiation transport model using the Green's function technique is being developed.*

## **INTRODUCTION**

The exposure of space travelers to radiation is determined in part by the transport properties of the radiation throughout the spacecraft, such as its onboard systems and the bodies of the individuals themselves. Meeting the challenge of future space programs will therefore require accurate and efficient methods for performing radiation transport calculations to determine and verify shielding requirements. According to a recent National Research Council Report [1], predictions derived from radiation transport calculations need to be tested using a common code for laboratory and space measurements that has been validated with accelerator results. Studies by Wilson et al. [2,3] have identified Green's function techniques as the likely means of generating efficient high charge and energy (HZE) shielding codes that are suitable for space engineering and are capable of being validated in laboratory experiments. In particular, the Green's function approach has the advantage of high computational efficiency compared to Monte Carlo codes in both laboratory and space simulations. Consequently, a laboratory code designed to simulate the transport of heavy ions through a single layer of material was developed [2,4]. It was based on a Green's function model as a perturbation series with non-perturbative corrections. The code was validated for single layer targets and then extended to handle multi-

layer targets [5,6,7]. This early code used a scale factor to equate range-energy relations of one material thickness into an equivalent amount of another material, and proceeded to perform the transport calculations in the new material [8]. While this method has proven to be acceptable using low-resolution detectors [6,9], it is not the most accurate reflection of different material properties and is not well suited for high-resolution measurements. Range and energy straggling, multiple Coulomb scattering, and energy downshift and dispersion associated with nuclear events were lacking from prior solutions. In recent publications [10,11], it has been shown how these effects can be incorporated into the multiple fragmentation perturbation series leading to the development of a new Green's function code GRNTRN (a GReeN's function code for ion beam TRaNsport). GRNTRN has proven to be accurate in modeling ion beams for a single layer of material [9,12], and has been extended to handle multiple layers [13]. Unlike the earlier Green's function code, the multi-layer GRNTRN code does not make use of range scaling, but instead transports ions through the target layer by layer. It is, however, a purely one dimensional code and does not take the variation of particle flux with angle into account. In order to remove this deficiency, it will be necessary to develop a fully three dimensional GRNTRN code. In this work, the progress made toward developing a fully three dimensional version of GRNTRN is reported.

## **TRANSPORT THEORY**

Consideration is given to the transport of high charge and energy ions through a three-dimensional convex region  $V$ , which is bounded by a smooth surface  $\partial V$ , and is filled with a target material. According to Wilson [14], the transport process is governed by the continuous slowing down, linear Boltzmann equation

$$\begin{aligned}
& \boldsymbol{\Omega} \cdot \nabla \phi_j(\mathbf{x}, \boldsymbol{\Omega}, E) - \partial_E \{ \tilde{S}_j(E) \phi_j(\mathbf{x}, \boldsymbol{\Omega}, E) \} + \sigma_j(E) \phi_j(\mathbf{x}, \boldsymbol{\Omega}, E) \\
& = \sum_{k>j}^N \int_{4\pi} d\Omega' \int_E^\infty dE' \sigma_{jk}(\boldsymbol{\Omega}, \boldsymbol{\Omega}', E, E') \phi_k(\mathbf{x}, \boldsymbol{\Omega}', E'),
\end{aligned} \tag{1}$$

with a boundary condition of the form

$$\phi_j(\mathbf{x}_b, \boldsymbol{\Omega}, E) = F_j(\mathbf{x}_b, \boldsymbol{\Omega}, E), \tag{2}$$

where  $\mathbf{x}_b$  is a point on the boundary, and  $N$  is the number of ions being transported. In equation (2), and throughout the rest of this paper, it is assumed that all boundary particles are directed inward towards the volume. In equations (1) and (2),  $F_j(\mathbf{x}_b, \boldsymbol{\Omega}, E)$  is a prescribed function,  $\phi_j(\mathbf{x}, \boldsymbol{\Omega}, E)$  is the flux of  $j$ -type ions with atomic mass  $A_j$  at position  $\mathbf{x}_b$  moving in the direction  $\boldsymbol{\Omega}$  with kinetic energy  $E$ ,  $\sigma_j(E)$  is the macroscopic absorption cross section,  $\tilde{S}_j(E)$  is the ion stopping power, and  $\sigma_{jk}(\boldsymbol{\Omega}, \boldsymbol{\Omega}', E, E')$  is the double differential production cross section for interactions in which  $j$ -type ions with energy  $E$  and direction  $\boldsymbol{\Omega}$  are produced by  $k$ -type ions with energy  $E'$  and direction  $\boldsymbol{\Omega}'$ . Throughout this paper, the units of energy will be expressed in MeV/amu, and units of depth in  $\text{g}/\text{cm}^2$ . The latter is obtained by multiplying the linear depth in cm by the volumetric density of the material in  $\text{g}/\text{cm}^3$ . Unless otherwise stated, all energies are kinetic.

The method of characteristics can be used to show that the Boltzmann equation and its boundary condition are equivalent to the transport integral equation [14]

$$\begin{aligned}
\phi_j(\mathbf{x}, \boldsymbol{\Omega}, E) & = \frac{P_j(\bar{E}_j) \tilde{S}_j(\bar{E}_j)}{P_j(E) \tilde{S}_j(E)} F_j[\mathbf{x}'(\mathbf{x}, \boldsymbol{\Omega}), \boldsymbol{\Omega}, \bar{E}_j] \\
& + \sum_{k>j}^N \int_{\rho'}^\rho \frac{P_j(E'') \tilde{S}_j(E'') d\rho''}{P_j(E) \tilde{S}_j(E)} \\
& \cdot \int_{E''}^\infty dE' \int_{4\pi} d\Omega' \sigma_{jk}(\boldsymbol{\Omega}, \boldsymbol{\Omega}', E'', E') \phi_k(\mathbf{x}_n + \rho'' \boldsymbol{\Omega}, \boldsymbol{\Omega}', E'),
\end{aligned} \tag{3}$$

where  $\rho \equiv \mathbf{x} \cdot \boldsymbol{\Omega}$  is the projection of the position vector onto the direction vector,  $\mathbf{x}_n \equiv \mathbf{x} - \rho \boldsymbol{\Omega}$  is an intermediate vector, and  $\mathbf{x}' \equiv \mathbf{x}_n + \rho' \boldsymbol{\Omega}$  is the point where the ray through  $\mathbf{x}$  in the direction  $\boldsymbol{\Omega}$  enters  $V$ . The term  $R_j(E)$  is the range of a  $j$ -type ion with energy  $E$ , and the residual energies

$$\bar{E}_j \equiv R_j^{-1}[R_j(E) + \rho - \rho'], \quad (4)$$

$$E'' \equiv R_j^{-1}[R_j(E) + \rho - \rho''], \quad (5)$$

are obtained through the usual range-energy relationship. Lastly, the nuclear survival probability,  $P_j(E)$ , is defined as

$$P_j(E) \equiv \exp \left[ - \int_0^E \frac{\sigma_j(H)}{\tilde{S}_j(H)} dH \right]. \quad (6)$$

By introducing the field vector  $\Phi(\mathbf{x}, \boldsymbol{\Omega}, E)$ , whose components are the  $j$ -type particle fluxes  $\phi_j(\mathbf{x}, \boldsymbol{\Omega}, E)$ , and following the procedure described in [10], the transport integral equation may be expressed in the operator form as

$$\Phi = \mathbf{G}^0 \cdot \mathbf{F} + \mathbf{Q} \cdot \mathbf{L} \cdot \Xi \cdot \Phi. \quad (7)$$

Since equation (7) is a Volterra type integral equation, it admits the Neumann series solution [10]

$$\begin{aligned} \Phi &= [\mathbf{G}^0 + (\mathbf{Q} \cdot \mathbf{L} \cdot \Xi) \cdot \mathbf{G}^0 + (\mathbf{Q} \cdot \mathbf{L} \cdot \Xi)^2 \cdot \mathbf{G}^0 + (\mathbf{Q} \cdot \mathbf{L} \cdot \Xi)^3 \cdot \mathbf{G}^0 + \dots] \cdot \mathbf{F} \\ &= [\mathbf{G}^0 + \mathbf{G}^1 + \mathbf{G}^2 + \mathbf{G}^3 + \dots] \cdot \mathbf{F}, \end{aligned} \quad (8)$$

where  $\mathbf{F}$  is the boundary flux vector whose components are the  $j$ -type boundary fluxes  $F_j$ . The term  $\mathbf{G}^n$  for  $n = 0, 1, 2, 3, \dots$  appearing in this expansion is called the  $n^{\text{th}}$  order Green's operator and is associated with the  $n^{\text{th}}$  generation of fragments produced. The above formalism lends to the following interpretation of the Neumann series. In the first term,  $\mathbf{G}^0 \cdot \mathbf{F}$ , the operator  $\mathbf{G}^0$  propagates primary ions from the boundary to the point  $\mathbf{x}$  with attenuation processes. In the

second term,  $\mathbf{Q} \cdot \mathbf{L} \cdot \mathbf{\Xi} \cdot \mathbf{G}^0 \cdot \mathbf{F}$ , the operator  $\mathbf{G}^0$  propagates primary ions from the boundary to an interior point  $\mathbf{x}''$  where a nuclear event takes place. The term  $\mathbf{\Xi} \cdot \mathbf{G}^0 \cdot \mathbf{F}$  is the production density of first generation secondaries at position  $\mathbf{x}''$ . These ions are transported from  $\mathbf{x}''$  to  $\mathbf{x}$  by the linear transport operator  $\mathbf{L}$ . Lastly, the quadrature operator,  $\mathbf{Q}$ , sums up all of the first generation fragments that are produced at interior points and transported to the point  $\mathbf{x}$ . The remaining terms of the Neumann series may be interpreted in a similar way and, from the series, the  $n^{\text{th}}$  order Green's operator can be computed recursively for  $n \geq 1$  as

$$\mathbf{G}^n = (\mathbf{Q} \cdot \mathbf{L} \cdot \mathbf{\Xi}) \cdot \mathbf{G}^{n-1}. \quad (9)$$

When the boundary condition (2) takes the special form

$$\phi_j(\mathbf{x}_b, \mathbf{\Omega}, E) = \frac{\delta_{jm}}{2\pi} \delta(1 - \mathbf{\Omega} \cdot \mathbf{\Omega}_0) \delta(E - E_0) \bar{\delta}(\mathbf{x}_b - \mathbf{x}_0), \quad (10)$$

where  $\bar{\delta}$  is the surface delta function on the boundary, the solution of equation (1) is called the Green's function and is denoted by the symbol  $G_{jm}(\mathbf{x}, \mathbf{x}_0, \mathbf{\Omega}, \mathbf{\Omega}_0, E, E_0)$ . Once the Green's function is known, the solution for an arbitrary boundary condition, as in equation (2), can be obtained from the formula

$$\begin{aligned} \phi_j(\mathbf{x}, \mathbf{\Omega}, E) &= [\mathbf{G} \cdot \mathbf{F}]_j(\mathbf{x}, \mathbf{\Omega}, E) = [(\mathbf{G}^0 + \mathbf{G}^1 + \mathbf{G}^2 + \mathbf{G}^3 + \dots) \cdot \mathbf{F}]_j(\mathbf{x}, \mathbf{\Omega}, E) \\ &= \sum_{k \geq j} \int_{\partial V} d\mathbf{x}_0 \int_{4\pi} d\Omega_0 \int_E^\infty dE_0 G_{jk}(\mathbf{x}, \mathbf{x}_0, \mathbf{\Omega}, \mathbf{\Omega}_0, E, E_0) F_k(\mathbf{x}_0, \mathbf{\Omega}_0, E_0). \end{aligned} \quad (11)$$

The summation is taken over  $k \geq j$  (instead of  $k > j$ ) to account for the primary ion spectrum.

## ZERO ORDER GREEN'S FUNCTION

The zero order Green's function is the first term in the Neumann series (8) with the unit boundary condition (10). When taking energy straggling in to account, as described in [10] and [11], it can be shown that the zero order Green's function takes the form

$$G_{jm}^0(\mathbf{x}, \mathbf{x}_0, \boldsymbol{\Omega}, \boldsymbol{\Omega}_0, E, E_0) = \frac{P_m(\bar{E}_m)}{P_m(E)} \frac{\delta_{jm}}{2\pi} \delta(1 - \boldsymbol{\Omega} \cdot \boldsymbol{\Omega}_0) \delta(\mathbf{x}' - \mathbf{x}_0) \cdot \frac{1}{\sqrt{2\pi} s_m(\rho - \rho', E_0)} \exp\left\{-\frac{[E - \hat{E}_m(\rho - \rho', E_0)]^2}{2 s_m(\rho - \rho', E_0)^2}\right\}, \quad (12)$$

where  $P_m(E)$  is the survival probability for  $m$ -type ions of energy  $E$ , and the residual energy is

$$\bar{E}_m \equiv R_m^{-1}[R_m(E) + \rho - \rho']. \quad (13)$$

The term

$$\hat{E}_m(\rho - \rho', E_0) \equiv R_m^{-1}[R_m(E_0) - (\rho - \rho')], \quad (14)$$

is the mean energy at depth  $(\rho - \rho')$  of an  $m$ -type ion that entered the transport material with kinetic energy  $E_0$ , and  $s_m(\rho - \rho', E_0)$  is the corresponding energy straggling width.

When the boundary condition takes a more general form, as in equation (2), the primary flux is obtained by integrating the zero order Green's function over all energies and directions within the volume

$$\begin{aligned} \phi_j^0(\mathbf{x}, \boldsymbol{\Omega}, E) &= [\mathbf{G}^0 \cdot \mathbf{F}]_j(\mathbf{x}, \boldsymbol{\Omega}, E) \\ &= \int_{\partial V} d\mathbf{x}_0 \int_{4\pi} d\boldsymbol{\Omega}_0 \int_E^\infty dE_0 G_{jj}^0(\mathbf{x}, \mathbf{x}_0, \boldsymbol{\Omega}, \boldsymbol{\Omega}_0, E, E_0) F_j(\mathbf{x}_0, \boldsymbol{\Omega}_0, E_0), \end{aligned} \quad (15)$$

which, in general, has to be evaluated numerically. In the accelerator beam model described below, equation (15) can be approximated analytically and a closed form expression may be obtained for the zero order primary flux. The result obtained in this case is called the broad zero order Green's function.

Since ion beam experiments play an important role in analyzing the shielding requirements against space radiations, modeling the propagation of accelerator beams through potential shielding materials is of interest. A simple model can be constructed by assuming that the accelerator beam consists of mono-energetic  $m$ -type particles of energy  $E_0$ , that move in the

direction  $\mathbf{\Omega}_0$  and enter the material at the point  $\mathbf{x}_0$  on its boundary. In this case, the boundary condition is given by equation (10), and the solution is the Green's function. In practice, however, the accelerator beam is neither mono-energetic nor unidirectional, and it enters the material at several points that are clustered about the mean value  $\mathbf{x}_0$ . A more realistic model can therefore be obtained by assuming that the beam has Gaussian profiles in both angle and energy, and that it enters the material at points that are distributed in a Gaussian manner about the mean point of entry,  $\mathbf{x}_0$ . In order to accomplish this, we will assume that the boundary is defined by the single-valued, continuously differentiable parametric equations  $\partial V \equiv \{\mathbf{x} : \mathbf{x} = \mathbf{x}(u, v)\}$ , with the bounds for  $u$  and  $v$  given by  $u_s \leq u \leq u_f$ ,  $v_s \leq v \leq v_f$ . In this case, the element of surface area is given by  $dS \equiv |\partial_u \mathbf{x} \times \partial_v \mathbf{x}| du dv$ . Further, at a non-singular point,  $\mathbf{x}_0 = \mathbf{x}_0(u_0, v_0)$ , of the parametric coordinate system, the surface delta function is denoted by  $\bar{\delta}$  and is given by

$$\bar{\delta}(\mathbf{x} - \mathbf{x}_0) = |\partial_u \mathbf{x}_0 \times \partial_v \mathbf{x}_0|^{-1} \delta(u - u_0) \delta(v - v_0). \quad (16)$$

The boundary condition (2) may then be assumed to take the Gaussian form

$$F_j(\mathbf{x}_b, \mathbf{\Omega}, E) = \frac{\delta_{jm} H[-\mathbf{\Omega} \cdot \mathbf{n}(\mathbf{x}_b)]}{4\pi s_x^2 s_\Omega s_E K_x K_\Omega |\partial_u \mathbf{x}_b \times \partial_v \mathbf{x}_b|} \exp\left\{-\frac{(u_b - u_0)^2 + (v_b - v_0)^2}{2s_x^2}\right\} \cdot \exp\left\{-\frac{(1 - \mathbf{\Omega} \cdot \mathbf{\Omega}_0)^2}{2s_\Omega^2}\right\} \exp\left\{-\frac{(E - E_0)^2}{2s_E^2}\right\}, \quad (17)$$

where  $\mathbf{x}_b = \mathbf{x}_b(u_b, v_b)$ ,  $H[x]$  is the Heaviside Function, and  $s_x$ ,  $s_\Omega$ , and  $s_E$  are the spreads in space, angle and energy, respectively. The normalization constants  $K_\Omega$  and  $K_x$  are given by

$$K_{\Omega} \equiv \pi \operatorname{erf} \left( \frac{\sqrt{2}}{s_{\Omega}} \right), \quad (18)$$

$$K_x \equiv \frac{1}{4} \left[ \operatorname{erf} \left( \frac{u_f - u_0}{\sqrt{2s_x}} \right) - \operatorname{erf} \left( \frac{u_s - u_0}{\sqrt{2s_x}} \right) \right] \left[ \operatorname{erf} \left( \frac{v_f - v_0}{\sqrt{2s_x}} \right) - \operatorname{erf} \left( \frac{v_s - v_0}{\sqrt{2s_x}} \right) \right], \quad (19)$$

where erf refers to the error function. It should be observed that in the limit as  $s_x, s_{\Omega}, s_E \rightarrow 0$ , the boundary condition (17) reduces to the Green's function boundary condition (10).

Equations (12) and (17) may now be substituted into equation (15) and the resulting integrals approximated by the mean value theorem and saddle point techniques discussed in [10]. The primary flux, which in this case is called the broad zero order Green's function,  $G_{jm}^b(\mathbf{x}, \mathbf{x}_0, \boldsymbol{\Omega}, \boldsymbol{\Omega}_0, E, E_0)$ , is then given by the expression

$$G_{jm}^b(\mathbf{x}, \mathbf{x}_0, \boldsymbol{\Omega}, \boldsymbol{\Omega}_0, E, E_0) \approx \frac{\delta_{jm} H[-\boldsymbol{\Omega} \cdot \mathbf{n}(\mathbf{x}')] \frac{P_m(\bar{E}_m)}{P_m(E)}}{4\pi K_x K_{\Omega} |\partial_u \mathbf{x}' \times \partial_v \mathbf{x}'| s_x^2 s_{\Omega} s_m^b(\rho - \rho', E_0)} \cdot \exp \left\{ -\frac{(u' - u_0)^2 + (v' - v_0)^2}{2s_x^2} \right\} \exp \left\{ -\frac{(1 - \boldsymbol{\Omega} \cdot \boldsymbol{\Omega}_0)^2}{2s_{\Omega}^2} \right\} \cdot \exp \left\{ -\frac{[E - \hat{E}_m(\rho - \rho', E_0)]^2}{2s_m^b(\rho - \rho', E_0)^2} \right\}, \quad (20)$$

where the residual energy is

$$\bar{E}_m \equiv \bar{E}_m(\rho - \rho', E) = R_m^{-1}[R_m(E) + \rho - \rho'], \quad (21)$$

and the broad energy spectral width is

$$s_m^b(\rho - \rho', E_0)^2 \equiv s_m(\rho - \rho', E_0)^2 + \left( \frac{\tilde{S}_m[\hat{E}_m(\rho - \rho', E_0)]}{\tilde{S}_m[E_0]} \right)^2 s_E^2. \quad (22)$$

Another simple case in which equation (15) can be approximated in closed form is that in which the boundary flux is uniform, isotropic and has a Gaussian energy profile. The primary

flux for this case is obtained by integrating equation (20) over all boundary points  $\mathbf{x}_0$  and all directions  $\mathbf{\Omega}_0$ . This yields the expression

$$\phi_j^0(\mathbf{x}, \mathbf{\Omega}, E) = \frac{\delta_{jm} H[-\mathbf{\Omega} \cdot \mathbf{n}(\mathbf{x}')] P_m(\bar{E}_m)}{\sqrt{2\pi} s_m^b(\rho - \rho', E_0) P_m(E)} \exp \left\{ -\frac{[E - \hat{E}_m(\rho - \rho', E_0)]^2}{2 s_m^b(\rho - \rho', E_0)^2} \right\}. \quad (23)$$

By way of illustration, the case is considered in which the target is an aluminum half-space,  $z \geq 0$ , whose boundary is exposed to a uniform, isotropic flux of  $^{56}\text{Fe}$  ions with a Gaussian energy profile having mean energy  $E_0 = 1000$  MeV/amu and energy width  $s_E = 10$  MeV/amu. In view of the geometry of this problem, it is convenient to describe the unit direction vector,  $\mathbf{\Omega}$ , by the spherical polar coordinates  $(1, \gamma, \alpha)$  that are related to its Cartesian components via the equation

$$\mathbf{\Omega} = \begin{pmatrix} \Omega_1 \\ \Omega_2 \\ \Omega_3 \end{pmatrix} = \begin{pmatrix} \sin \gamma \cos \alpha \\ \sin \gamma \sin \alpha \\ \cos \gamma \end{pmatrix}, \quad (24)$$

where  $\alpha$  is the polar angle and  $\gamma$  is the inclination angle. Since there is axial symmetry about the  $z$ -direction, results are presented only for the case in which  $\alpha = 0$  deg.

Figures 1-3 show the primary flux as a function of inclination angle,  $\gamma$ , and energy at depths  $z = 0, 5, \text{ and } 15$  g/cm<sup>2</sup> of aluminum when  $\alpha = 0$  deg. The attenuation with angle and depth is clearly shown as is the increasing variation with angle at greater depths.

## THE PRODUCTION CROSS SECTIONS

Before constructing the first order Green's function, it will be necessary to obtain an expression for the double differential production cross sections,  $\sigma_{jk}(\mathbf{\Omega}, \mathbf{\Omega}_k, E, E_k)$ . The production cross section,  $\sigma_{jk}(\mathbf{\Omega}, \mathbf{\Omega}_k, E, E_k)$ , is for fragments of mass  $A_j$  moving in the direction

$\Omega$  with kinetic energy  $E$  that are produced when projectiles of mass  $A_k$  moving in the direction  $\Omega_k$  with kinetic energy  $E_k$  strike a target. In the analysis to follow, a tilde ( $\tilde{\phantom{x}}$ ) will be used to distinguish between kinetic energy and total energy. Thus, if a particle has kinetic energy  $E$ , its total energy will be denoted by  $\tilde{E} = E + m_p$ , where  $m_p = 938.272$  MeV is the proton rest mass.

The nuclear fragmentation cross section can be expressed in the form

$$\frac{d^3\sigma_{jk}}{dp^3} = \sigma_{jk}(E_k)f_{jk}(\mathbf{p}), \quad (25)$$

where  $\sigma_{jk}(E_k)$  is the total cross section, and  $f_{jk}(\mathbf{p})$  the fragment momentum distribution. Experiments show that when fragments are produced, they may be projectile-like or target-like. This implies that the fragments have small momenta in their respective rest frames. It has been determined that the momentum distributions of these fragments can be well approximated by Gaussians in reference frames close to their respective rest frames. Here, it is assumed that the distributions are Gaussian in the frame where the average fragment momentum is zero. Quantities evaluated in this frame will be denoted with the symbol  $*$  to distinguish them from their counterparts in the laboratory frame.

According to Townsend et al. [15], it may be assumed that the fragmentation is isotropic in the  $*$  frame, in which case the momentum distribution may be expressed as

$$f_{jk}^*(\mathbf{p}^*) \approx \frac{1}{(2\pi)^{\frac{3}{2}}\sigma^3} \exp\left(-\frac{p^{*2}}{2\sigma^2}\right), \quad (26)$$

where  $\mathbf{p}^* = \mathbf{p}_\perp^* + \mathbf{p}_\parallel^*$ , and the terms  $\mathbf{p}_\perp^*$  and  $\mathbf{p}_\parallel^*$  are the fragment's momentum transverse and parallel to the beam. The momentum width,  $\sigma$ , is given by Tripathi et al. [16] as

$$\sigma \equiv \frac{1}{A_j} \sqrt{\frac{m_p}{2} \left( \frac{45}{A_k^{\frac{1}{3}}} - \frac{25}{A_k^{\frac{2}{3}}} \right) \left( \frac{A_j (A_k - A_j)}{A_j - 1} \right)}. \quad (27)$$

On transforming to the lab frame, while keeping in mind that  $f_{jk}$  transforms like  $\frac{1}{dp^3}$  and that  $\frac{\tilde{E}}{dp^3}$  is Lorentz invariant, it is found that

$$f_{jk}(\mathbf{p}) \approx \frac{\tilde{E}^*}{\tilde{E}} \frac{1}{(2\pi)^2 \sigma^3} \exp\left(-\frac{p^{*2}}{2\sigma^2}\right). \quad (28)$$

In equation (28),  $\tilde{E}^* \equiv \gamma_L(\tilde{E} - \beta_L p_{\parallel})$ ,  $p_{\parallel}^* \equiv \gamma_L(p_{\parallel} - \beta_L \tilde{E})$ ,  $p_{\perp}^* = p_{\perp}$ , and  $\beta_L \equiv \sqrt{1 - \gamma_L^{-2}}$ .

The Lorentz factors, are given by  $\gamma_L \equiv \frac{\tilde{E}_k - E_s}{m_p}$  for projectile-like fragments and  $\gamma_L \equiv \frac{E_s}{m_p}$

for target-like fragments. The term  $E_s = E_s(E_k)$  is the lab frame energy shift which is determined as follows.

According to Tripathi et al. [16], the projectile frame momentum shift is given by

$$P_s^* = \frac{1}{A_j} \left[ 3.64 \left( 9 + \frac{A_j}{A_k} \right) \sqrt{\frac{9}{A_k^{1/3}} - \frac{5}{A_k^{2/3}} - 28} \right], \quad (29)$$

and the corresponding energy shift by  $\sqrt{P_s^{*2} + m_p^2} - m_p$ . On transforming to the lab frame it is found that

$$E_s = \gamma_k \left[ \sqrt{P_s^{*2} + m_p^2} - m_p + \beta_k P_s^* \right], \quad (30)$$

where  $\gamma_k \equiv \frac{\tilde{E}_k}{m_p}$  and  $\beta_k \equiv \sqrt{1 - \gamma_k^{-2}}$ .

Let  $\theta = \cos^{-1}(\mathbf{\Omega} \cdot \mathbf{\Omega}_k)$  be the lab scattering angle and let  $(p, \theta, \phi)$  be spherical polar coordinates with polar axis in the incident beam direction,  $\mathbf{\Omega}_k$ . Then,  $p_{\perp} = p \sin \theta$  and  $p_{\parallel} = p \cos \theta$ , where  $p = \sqrt{\tilde{E}^2 - m_p^2}$ . Since there is axial symmetry,

$$\begin{aligned}
\sigma_{jk}(\mathbf{\Omega}, \mathbf{\Omega}_k, E, E_k) d\Omega dE &= \sigma_{jk}(E_k) f_{jk}(\mathbf{p}) d^3 p \\
&= 2\pi \sigma_{jk}(E_k) f_{jk}(\mathbf{p}) p^2 \sin \theta dp d\theta \\
&= 2\pi \sigma_{jk}(E_k) f_{jk}(\mathbf{p}) p \sin \theta \tilde{E} dE d\theta \\
&= \sigma_{jk}(E_k) f_{jk}(\mathbf{p}) p \tilde{E} d\Omega dE,
\end{aligned} \tag{31}$$

showing that the production cross section is given by

$$\sigma_{jk}(\mathbf{\Omega}, \mathbf{\Omega}_k, E, E_k) = \sigma_{jk}(E_k) \frac{p(\tilde{E}) \tilde{E}^*[\tilde{E}, \theta]}{(2\pi)^2 \sigma^3} \exp\left(-\frac{\tilde{E}^*[\tilde{E}, \theta]^2 - m_p^2}{2\sigma^2}\right), \tag{32}$$

where

$$\tilde{E}^*[\tilde{E}, \theta] = \gamma_L [\tilde{E} - \beta_L \sqrt{\tilde{E}^2 - m_p^2} \cos \theta]. \tag{33}$$

Since the exponential appearing in equation (32) achieves its maximum when  $\tilde{E} = \gamma m_p$  and  $\theta = 0$ , a useful simplification can be obtained by expanding about this point in powers of the parameters  $\varepsilon$  and  $\mu$  that are defined by  $\varepsilon \equiv \tilde{E} - \gamma m_p$ ,  $\mu \equiv 1 - \cos \theta$ . By retaining terms up to second order, it can then be shown that

$$\sigma_{jk}(\mathbf{\Omega}, \mathbf{\Omega}_k, E, E_k) \approx \sigma_{jk}(E_k) f_E(E, E_k) f_{\Omega}(\mathbf{\Omega}, \mathbf{\Omega}_k, E_k), \tag{34}$$

where

$$f_E(E, E_k) \approx \frac{1}{(2\pi)^2 \sigma \gamma_L \beta_L} \exp\left(-\frac{(E_k - E_s - E)^2}{2\sigma^2 \gamma_L^2 \beta_L^2}\right), \tag{35}$$

and

$$f_{\Omega}(\Omega, \Omega_k, E_k) = H[\pi/2 - \theta] \frac{\gamma_L^2 \beta_L^2 m_p^2 \cos \theta}{2\pi\sigma^2} \exp\left(-\frac{\gamma_L^2 \beta_L^2 m_p^2 \sin^2 \theta}{2\sigma^2}\right). \quad (36)$$

## FIRST ORDER GREEN'S FUNCTION

The next term in the Neumann Series that needs to be calculated is the first order Green's function, which represents the transport of first generation fragments. Since the Green's function boundary condition (10) is a special case of the broad Green's function boundary condition (17), we need only deal with the latter. It may be recalled that the first generation flux is given by the recurrence relation  $\Phi^1 = (\mathbf{Q} \cdot \mathbf{L} \cdot \Xi) \cdot \Phi^0$ . Therefore, on replacing  $\Phi^0$  by the broad zero order Green's function and expanding the result, the broad first order Green's function is given by expression

$$\begin{aligned} G_{jm}^1(\mathbf{x}, \mathbf{x}_0, \Omega, \Omega_0, E, E_0) &= \int_{\rho'}^{\rho} d\rho'' \int_{E''}^{\infty} dE_1 \int_{4\pi} d\Omega_1 \\ &\cdot \frac{P_j(E'') \tilde{S}_j(E'')}{P_j(E) \tilde{S}_j(E)} \sigma_{jm}(\Omega, \Omega_1, E'', E_1) \\ &\cdot \frac{H[-\Omega_1 \cdot \mathbf{n}(\mathbf{x}_1')] P_m[\bar{E}_m(\rho_1'' - \rho_1', E_1)]}{4\pi K_x K_{\Omega} |\partial_u \mathbf{x}_1' \times \partial_v \mathbf{x}_1'| s_x^2 s_{\Omega} s_m^b(\rho_1'' - \rho_1', E_0) P_m[E_1]} \\ &\cdot \exp\left\{-\frac{(u_1' - u_0)^2 + (v_1' - v_0)^2}{2s_x^2}\right\} \\ &\cdot \exp\left\{-\frac{(1 - \Omega_1 \cdot \Omega_0)^2}{2s_{\Omega}^2}\right\} \\ &\cdot \exp\left\{-\frac{[E_1 - \hat{E}_m(\rho_1'' - \rho_1', E_0)]^2}{2s_m^b(\rho_1'' - \rho_1', E_0)^2}\right\}, \end{aligned} \quad (37)$$

where  $\rho_1'' \equiv \mathbf{x}'' \cdot \Omega_1$  and  $\mathbf{x}_1' = \mathbf{x}'' - (\rho_1'' - \rho_1') \Omega_1$  is the point where the ray through  $\mathbf{x}''$ , in

the direction  $\Omega_1$  enters  $V$ . The residual energy is

$$\bar{E}_m(\rho_1'' - \rho_1', E_1) \equiv R_m^{-1}[R_m(E_1) + \rho_1'' - \rho_1'], \quad (38)$$

and the mean energy at depth  $(\rho_1'' - \rho_1')$  of an  $m$ -type ion that entered the transport material with energy  $E_0$  is

$$\hat{E}_m(\rho_1'' - \rho_1', E_0) \equiv R_m^{-1}[R_m(E_0) - (\rho_1'' - \rho_1')]. \quad (39)$$

The term  $s_m^b(\rho_1'' - \rho_1', E_0)$  is the broad spectrum energy width.

The expression in equation (37) can be evaluated by numerical quadrature, but this is computationally expensive. Therefore, it is desirable to construct an analytical approximation. This can be done by making use of Taylor's theorem, the mean value theorem, and saddle point techniques as described in [10]. This yields the result

$$\begin{aligned} G_{jm}^1(\mathbf{x}, \mathbf{x}_0, \mathbf{\Omega}, \mathbf{\Omega}_0, E, E_0) &= \frac{H[-\mathbf{\Omega} \cdot \mathbf{n}(\mathbf{x}')] }{(2\pi)^{\frac{3}{2}} K_x K_\Omega s_x^2 s_\Omega |\partial_u \mathbf{x}' \times \partial_v \mathbf{x}'|} \\ &\cdot \exp\left\{-\frac{(u' - u_0)^2 + (v' - v_0)^2}{2s_x^2}\right\} \exp\left\{-\frac{(1 - \mathbf{\Omega} \cdot \mathbf{\Omega}_0)^2}{2s_\Omega^2}\right\} \\ &\cdot \left[ \frac{C_{jm}(\rho^*)}{2g_{jm}'(\rho^*)} \left\{ \operatorname{erf}\left(\frac{g_{jm}(\rho)}{\sqrt{2}s_m^1(\rho^*)}\right) - \operatorname{erf}\left(\frac{g_{jm}(\rho')}{\sqrt{2}s_m^1(\rho^*)}\right) \right\} \right. \\ &\left. - \frac{C_{jm}'(\rho^*)s_m^1(\rho^*)}{\sqrt{2\pi}g_{jm}'(\rho^*)^2} \left\{ \exp\left(\frac{-g_{jm}(\rho)^2}{2s_m^1(\rho^*)^2}\right) - \exp\left(\frac{-g_{jm}(\rho')^2}{2s_m^1(\rho^*)^2}\right) \right\} \right], \end{aligned} \quad (40)$$

where  $\rho^*$  is the root of the equation  $g_{jm}(\rho'') = 0$ , and the other terms in equation (40) are given by the following

$$g_{jm}(\rho'') = \hat{E}_m(\rho'' - \rho, E_0) - E_s[\hat{E}_m(\rho'' - \rho, E_0)] - \bar{E}_j(\rho - \rho'', E), \quad (41)$$

$$s_m^1(\rho^*)^2 = s_m^b(\rho^* - \rho', E_0)^2 + \sigma^2 \gamma_L [\hat{E}_m(\rho - \rho^*, E_0)]^2 \beta_L [\hat{E}_m(\rho - \rho^*, E_0)]^2, \quad (42)$$

$$C_{jm}(\rho'') = \frac{P_j[\bar{E}_j(\rho - \rho'', E)] \tilde{S}_j[\bar{E}_j(\rho - \rho'', E)] P_m(E_0)}{P_j(E) \tilde{S}_j(E) P_m[\hat{E}_m(\rho - \rho'', E_0)]} \sigma_{jm}^r[\hat{E}_m(\rho - \rho'', E_0)], \quad (43)$$

$$\bar{E}_j(\rho - \rho'', E) = R_j^{-1}[R_j(E) + \rho - \rho''], \quad (44)$$

$$\hat{E}_m(\rho'' - \rho, E_0) = R_m^{-1}[R_m(E_0) - (\rho'' - \rho)]. \quad (45)$$

For the special case in which the boundary flux is uniform, isotropic and has a Gaussian energy profile, the first generation fragment flux is obtained by integrating equation (40) over all boundary points,  $\mathbf{x}_0$ , and all directions,  $\mathbf{\Omega}_0$ . This yields the result

$$\begin{aligned} \phi_j^1(\mathbf{x}, \mathbf{\Omega}, E) = & \frac{C_{jm}(\rho^*)}{2g_{jm}'(\rho^*)} \left\{ \operatorname{erf} \left( \frac{g_{jm}(\rho)}{\sqrt{2s_m^1(\rho^*)}} \right) - \operatorname{erf} \left( \frac{g_{jm}(\rho')}{\sqrt{2s_m^1(\rho^*)}} \right) \right\} \\ & - \frac{C_{jm}'(\rho^*)s_m^1(\rho^*)}{\sqrt{2\pi}g_{jm}'(\rho^*)^2} \left\{ \exp \left( \frac{-g_{jm}(\rho)^2}{2s_m^1(\rho^*)^2} \right) - \exp \left( \frac{-g_{jm}(\rho')^2}{2s_m^1(\rho^*)^2} \right) \right\}. \end{aligned} \quad (46)$$

Again, the results are illustrated for the aluminum half-space problem described above. Figures 4-6 show the secondary  $^{16}\text{O}$  fragment flux as a function of inclination angle,  $\gamma$ , and energy at depths  $z = 5, 10, \text{ and } 15 \text{ g/cm}^2$  of aluminum with an  $1000 \text{ MeV/amu } ^{56}\text{Fe}$  projectile. In these figures, at a depth of  $z = 5 \text{ g/cm}^2$ , the number of fragments are increasing with depth until  $\sim 80 \text{ deg}$  where a large decrease with depth occurs as the stopping range of the particle is approached. Close to the boundary, there are no fragments produced, which is why there is still an increase in fragments at a relatively shallow depth. The other two figures show that with increasing depth, the number of fragments decrease as the stopping range is approached.

As a verification of the approximations used, the first order fragment flux was computed by evaluating the integrals in equation (37) numerically. A comparison was then made between the numerical results and those obtained by analytical approximation. This comparison is shown in Figures 7-8 which exhibit the  $^{16}\text{O}$  fragment flux at depth  $z = 10 \text{ g/cm}^2$ . Figure 7 shows the variation of the fragment flux with inclination angle,  $\gamma$ , for several energy values and Figure 8 the variation of the fragment flux with energy for several values of the inclination angle,  $\gamma$ . Note

that there is good agreement between the results, indicating that the approximations used are accurate.

## RESULTS

In this work, analytical approximation techniques have been used to obtain closed form expressions for the first and second terms in the Neumann series solution of the three dimensional linear Boltzmann equation. Results were presented for the case in which a uniform, isotropic flux of  $^{56}\text{Fe}$  ions with a Gaussian energy profile strikes the boundary of an aluminum half-space. A comparison between the closed form results and comparable results obtained by numerical quadrature shows that the approximations used are accurate. In addition, while the numerical results presented took several hours to generate, the analytical results were obtained in a few seconds showing the feasibility of obtaining a fast and accurate three dimensional ion transport code.

The construction of the remaining terms of the Neumann series will be addressed in future work along with comparison to measured laboratory data. It is anticipated that an approximate closed form expression will be found for the second order Green's function and the series remainder obtained by a non-perturbative technique.

## NOMENCLATURE

$\Phi$  = Flux column vector

$\Omega$  = Direction of propagation

$Q$  = Quadrature operator

$L$  = Linear transport operator

$\Xi$  = Fragmentation or collision operator

$P_j(E)$  = Total survival probability

$\tilde{S}_j(E)$  = Energy lost per unit path length

$\sigma_j(E)$  = Macroscopic absorption cross section

$\sigma_{jk}(\Omega, \Omega', E, E')$  = Double differential production cross section

$\phi_k(\mathbf{x}, \Omega', E')$  = Flux of  $k$ -type ions

$m_p$  = Rest mass of a proton  $\gamma_L$  = Fragment Lorentz factor

$\beta_L$  = Fragment beta factor

$E_s$  = Fragment average energy downshift

$\sigma$  = Fragment momentum width

## REFERENCES

1. Committee on the Evaluation of Radiation Shielding for Space Exploration, *Managing Space Radiation Risk in the New Era of Space Exploration* (The National Academies Press, Washington, D.C., 2008).
2. J.W. Wilson, et al., *A closed form solution to HZE propagation*, (Radiat. Res., **122**, 223-228, 1990).
3. J. W. Wilson, et al., *A hierarchy of transport approximations for high energy heavy (HZE) ions*, (NASA TM-4118, National Aeronautics and Space Administration, 1989).
4. J. W. Wilson, et al., *Non-perturbative methods in HZE transport*, (NASA TP-3363, National Aeronautics and Space Administration, 1993).
5. J. W. Wilson, et al., *Transport Methods and Interactions for Space Radiations*, (NASA RP 1257, National Aeronautics and Space Administration, 1991).
6. J. L. Shinn, et al., *HZE beam Transport in Multilayered Materials*, (Radiat. Meas., **23**, 57-64, 1994).
7. J. L. Shinn, et al., *A Green's function method for heavy ion beam transport*, (Radiat. Environ. Biophys., **34**, 155-159, 1995).
8. J. L. Shinn, et al., *Multilayer analysis of an Iron radiation beam experiment*, (NASA TM-4753, National Aeronautics and Space Administration, 1997).
9. S. A. Walker, et al., *Validation of the HZETRN code for laboratory exposures with 1 A GeV iron ions in several targets*, (Adv. Space Res., **35**, 202-207, 2005).

10. J. Tweed, et al., *An improved Green's function for ion beam transport*, (Adv. Space Res., **34**, 1311-1318, 2004).
11. C. J. Mertens, et al. *Coupling of Multiple Coulomb Scattering with Energy Loss and Straggling in HZETRN*, (Adv. Space Res., **40**, 1357-1367, 2007).
12. J. Tweed, et al., *Validation Studies of the GRNTRN Code for Radiation Transport*, (ICES 2007-01-3118, SAE 37th International Conference on Environmental Systems, Chicago, 2007).
13. J. Tweed, et al., *Recent Progress in the Development of a Multi-Layer Green's Function Code for Ion Beam Transport*, (STAIF-2008 (Space Technology & Applications Forum), Albuquerque, NM, February 10-14, 2008. *AIP Conf. Proc.*, **969**, 993-100, 2008).
14. J. W. Wilson, *Analysis of the Theory of High-Energy Ion Transport*, (NASA TN D-8381, National Aeronautics and Space Administration, 1977).
15. L.W. Townsend, et al., *Optical model analyses of 1.65A GeV argon fragmentation: Cross sections and momentum distributions*, (Phys. Rev. C, **48**, 2912-2919, 1993).
16. R.K. Tripathi, et al., *Role of intrinsic width in fragment momentum distributions in heavy ion collisions*, (Phys. Rev. C, **49**, 1775-1777, 1994).

## FIGURE DESCRIPTIONS

Figure 1. The  $^{56}\text{Fe}$  primary ion flux at depth  $z = 0 \text{ g/cm}^2$  when  $\alpha = 0 \text{ deg}$ .

Figure 2. The  $^{56}\text{Fe}$  primary ion flux at depth  $z = 5 \text{ g/cm}^2$  when  $\alpha = 0 \text{ deg}$ .

Figure 3. The  $^{56}\text{Fe}$  primary ion flux at depth  $z = 15 \text{ g/cm}^2$  when  $\alpha = 0 \text{ deg}$ .

Figure 4. The  $^{16}\text{O}$  fragment flux at depth  $z = 5 \text{ g/cm}^2$  when  $\alpha = 0 \text{ deg}$ .

Figure 5. The  $^{16}\text{O}$  fragment flux at depth  $z = 10 \text{ g/cm}^2$  when  $\alpha = 0 \text{ deg}$ .

Figure 6. The  $^{16}\text{O}$  fragment flux at depth  $z = 15 \text{ g/cm}^2$  when  $\alpha = 0 \text{ deg}$ .

Figure 7. A comparison between the numerical and approximate  $^{16}\text{O}$  fragment fluxes at depth  $z = 10 \text{ g/cm}^2$  for several energies (MeV/amu).

Figure 8. A comparison between the numerical and approximate  $^{16}\text{O}$  fragment fluxes at depth  $z = 10 \text{ g/cm}^2$  for several inclination angles (deg).

# FIGURES

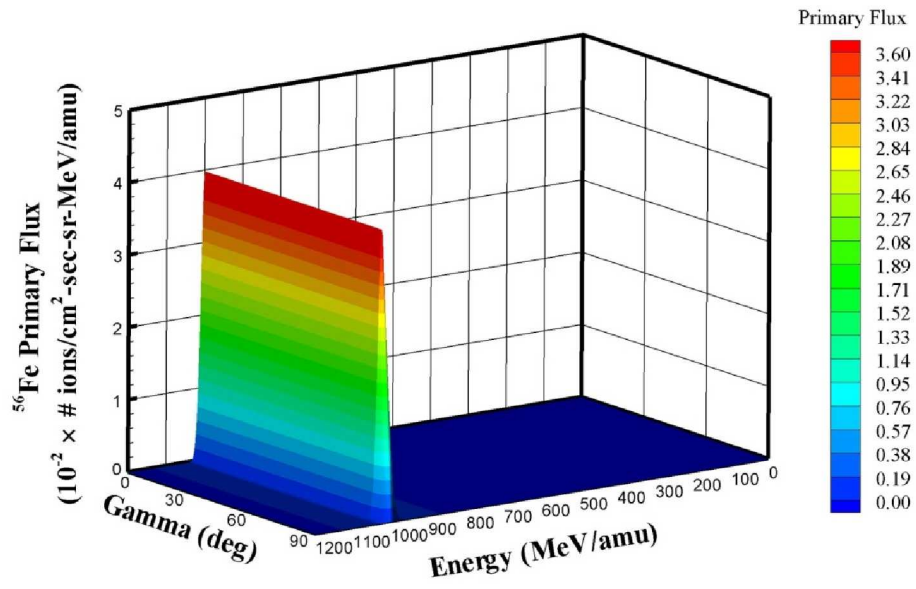


Figure 1

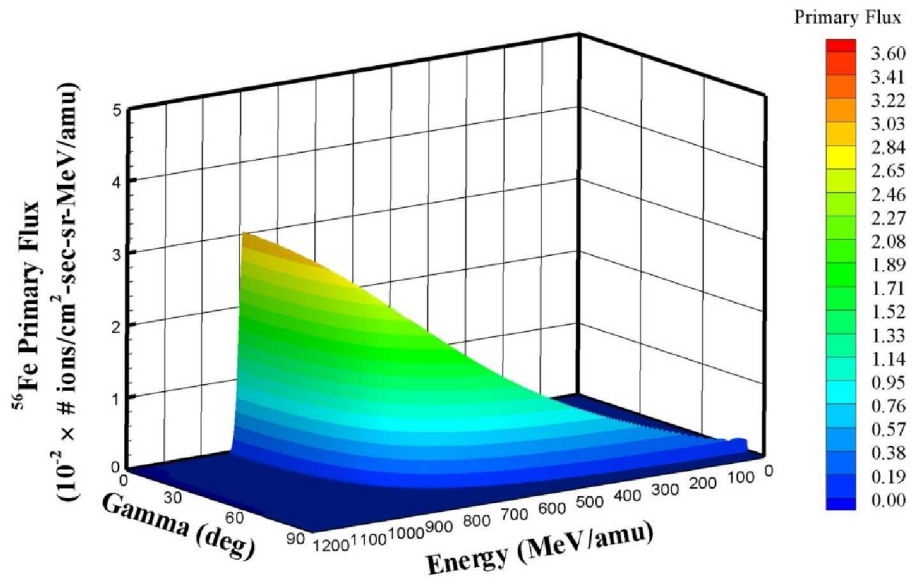


Figure 2

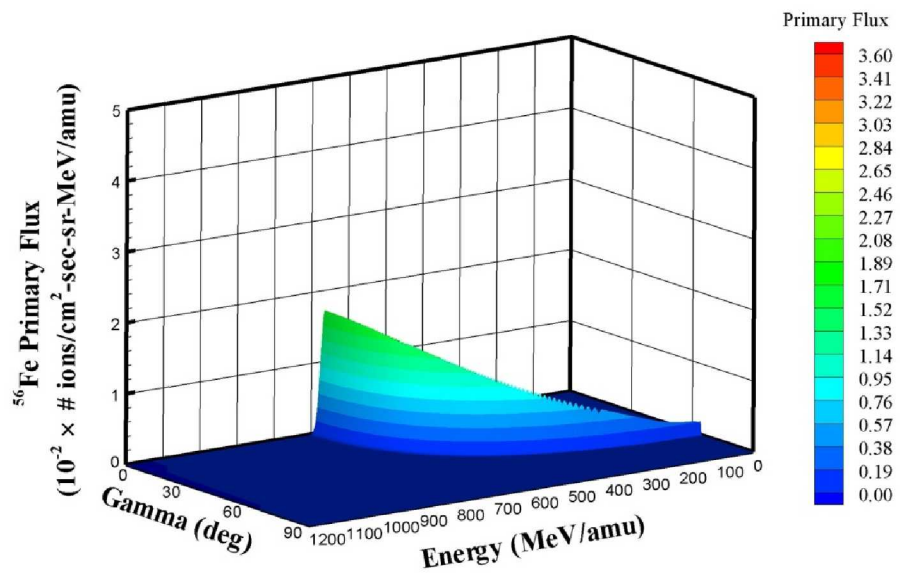


Figure 3

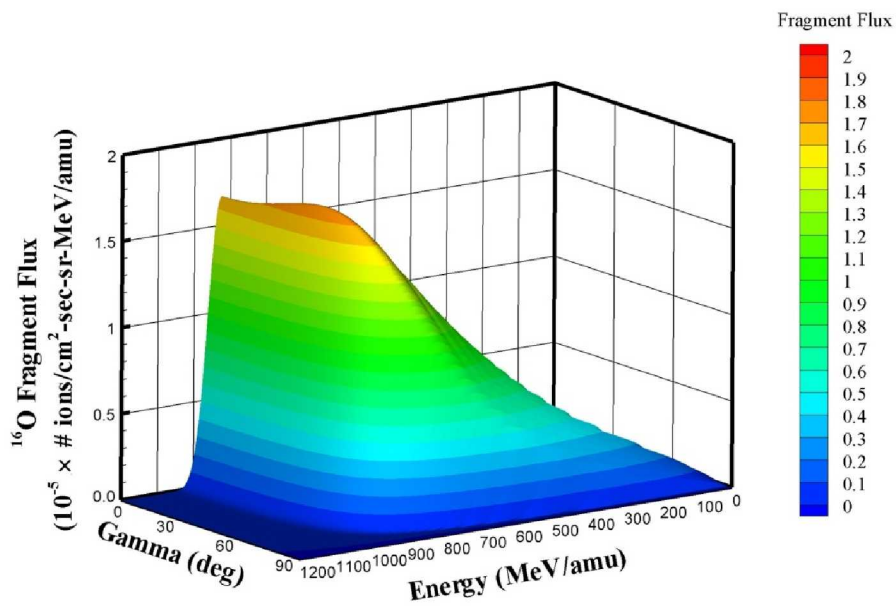


Figure 4

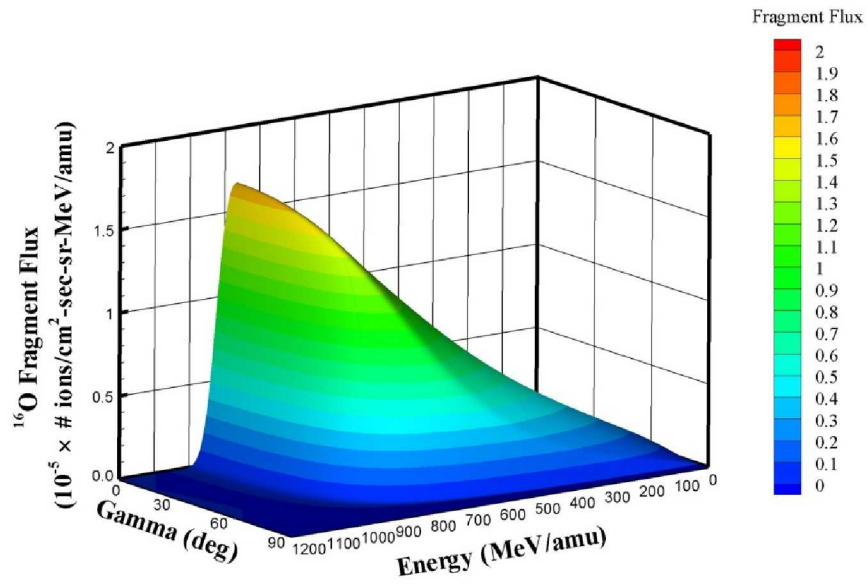


Figure 5

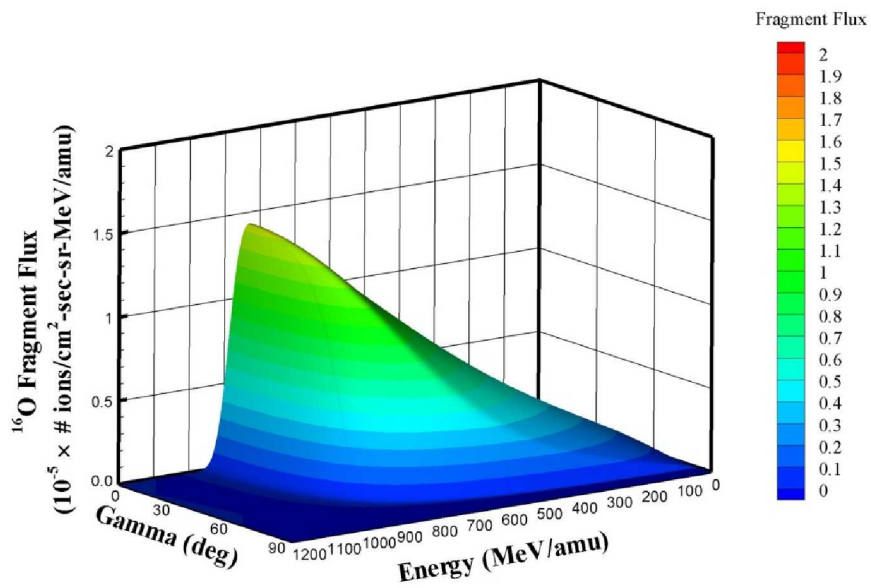


Figure 6

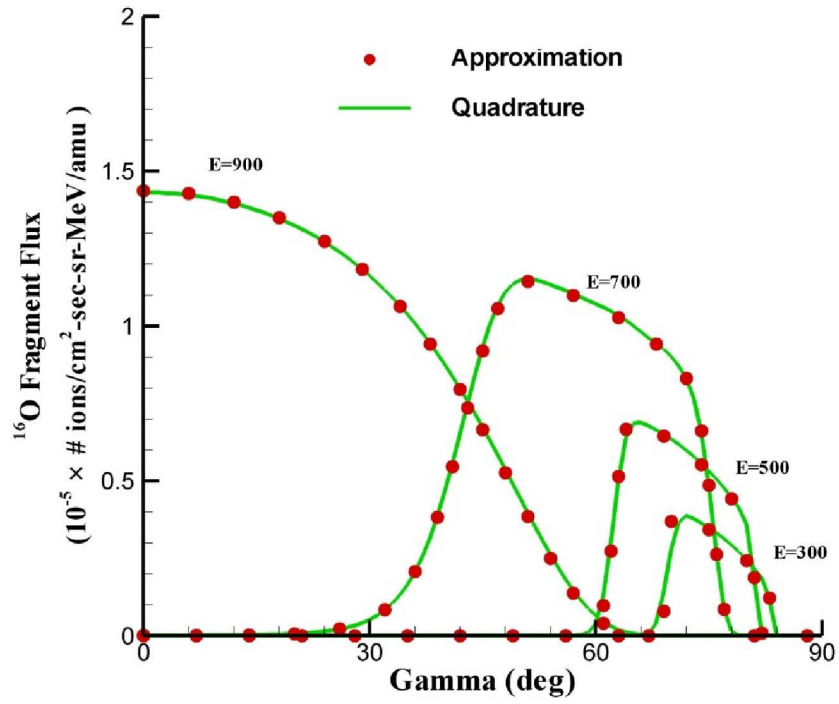


Figure 7

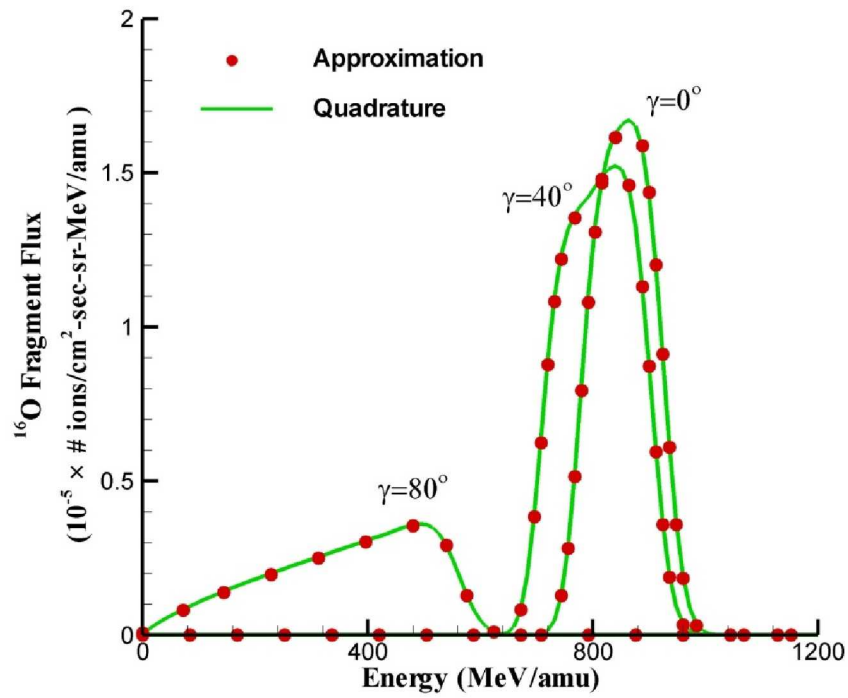


Figure 8